

Preliminary Investigation on the Geometric Accuracy of 3D Printed Dental Implant Using a Monkey Maxilla Incisor Model

Yuchun Liu^{1,2}, Swee Leong Sing³, Rebecca Xin En Lim¹, Wai Yee Yeong⁴, Bee Tin Goh^{1,2,5*}

¹National Dental Research Institute Singapore, National Dental Centre Singapore, Singapore

²Oral Health Academic Clinical Programme, Duke-NUS Medical School, Singapore

³Department of Mechanical Engineering, National University of Singapore, Singapore

⁴Singapore Centre for 3D Printing, School of Mechanical and Aerospace Engineering, Nanyang Technological University, Singapore

⁵Department of Oral and Maxillofacial Surgery, National Dental Centre Singapore, Singapore

Abstract: Additive manufacturing has proven to be a viable alternative to conventional manufacturing methodologies for metallic implants due to its capability to customize and fabricate novel and complex geometries. Specific to its use in dental applications, various groups have reported successful outcomes for customized root-analog dental implants in preclinical and clinical studies. However, geometrical accuracy of the fabricated samples has never been analyzed. In this article, we studied the geometric accuracy of a 3D printed titanium dental implant design against the tooth root of the monkey maxilla incisor. Monkey maxillas were scanned using cone-beam computed tomography, then segmentation of the incisor tooth roots was performed before the fabrication of titanium dental implants using a laser powder bed fusion (PBF) process. Our results showed $68.70\% \pm 5.63$ accuracy of the 3D printed dental implant compared to the actual tooth ($n = 8$), where main regions of inaccuracies were found at the tooth apex. The laser PBF fabrication process of the dental implants showed a relatively high level of accuracy of $90.59\% \pm 4.75$ accuracy ($n = 8$). Our eventual goal is to develop an accurate workflow methodology to support the fabrication of patient-specific 3D-printed titanium dental implants that mimic patients' tooth anatomy and fit precisely within the socket upon tooth extraction. This is essential for promoting primary stability and osseointegration of dental implants in the longer term.

Keywords: Additive manufacturing; 3D printing; Segmentation; Root-analog dental implant; Maxilla incisor; Monkey model; Computed tomography

*Correspondence to: Bee Tin Goh, National Dental Research Institute Singapore, National Dental Centre Singapore, Singapore; goh.bee.tin@singhealth.com.sg

Received: December 6, 2021; **Accepted:** January 10, 2022; **Published Online:** January 28, 2022

(This article belongs to the *Special Section: 3D Printing and Bioprinting for the Future of Healthcare*)

Citation: Liu Y, Sing SL, Lim RXE, et al., 2022, Preliminary Investigation on the Geometric Accuracy of 3D Printed Dental Implant Using a Monkey Maxilla Incisor Model. *Int J Bioprint*, 8(1): 476. <http://doi.org/10.18063/ijb.v8i1.476>

1. Introduction

With the recent advances in additive manufacturing (AM) or three-dimensional (3D) printing technology, there has been an increased popularity in their use for fabricating metallic implants for biomedical applications due to the ability to customize fabrication for personalized patient treatment^[1]. Complex geometries with tunable implant properties can now be fabricated^[2]. A good match of

the implant to the bone defect region can be customized through computer-aided design (CAD) based on patients' scans to achieve better bone integration^[3,4]. Other advantages of 3D printing include low costs, shorter manufacturing duration, and high consistency^[5].

Compared to conventional manufacturing methodologies where metallic implants are manufactured using formative techniques such as forging or casting,

and subtractive techniques like milling or machining^[6], AM produces parts from 3D digital data using the layer-by-layer process of joining raw materials. For implants, powder bed fusion (PBF) is the most established AM processes. In PBF, layers of powder are thermally fused using an energy source, which can be lasered in laser PBF (L-PBF) or electron beam in electron beam PBF (EB-PBF). L-PBF is also commonly referred to as selective laser melting (SLM) while EB-PBF is called electron beam melting.

L-PBF has the capability to produce highly complex metallic parts with densities and mechanical performance matching those from conventional methods^[7-9]. However, geometrical accuracy remains a challenge due to the multiple steps involved in the process chain of fabrication^[10,11]. Few groups have shown the feasibility of using L-PBF to manufacture root-analog dental implants for immediate implant placement^[12]. Moin *et al.* showed the feasibility of obtaining models using cone-beam computed tomography (CT) scan and the subsequent fabrication of the root analog implants (RAI) using L-PBF^[13,14]. Chen *et al.* evaluated the mechanical and biomechanical performance of customized dental implants fabricated by L-PBF. They obtained the digital files using reverse engineering by obtaining CT images of a maxillary incisor which are then used to create the customized RAI^[15]. Li *et al.* studied how the build orientation and scanning parameters affect the surface roughness of RAI fabricated using L-PBF. Based on their preliminary studies, they further analyzed the effect of using constant parameters and gradient parameters, meaning different parameters at different segments of the implants. It is found that using gradient parameters, consistent and low surface roughness can be obtained for the RAI^[16]. Li *et al.* produced RAI with oval cross-section abutment design using L-PBF; however, the designs are not obtained using imaging techniques. Nonetheless, they showed the potential of the material performance and feasibility of using L-PBF as the fabrication method^[17]. Similarly, Guo *et al.* studied the performance of RAI fabricated using L-PBF by finite element model simulations and verified them using actual fabricated samples, without consideration for the accuracy of the fabricated samples^[18]. A similar study was also conducted by Song *et al.*^[19].

The ideal customized dental implant should fit precisely within the socket for immediate implant placement upon tooth extraction. The immediate implant placement approach is advantageous over delayed implants as it significantly shortens overall treatment duration, reduces treatment costs, and preserves the bone and gingival tissues^[20]. Current conventional dental implants are machined into pre-determined sizes with a standard screw-form design, and the stability of the

implant at the time of placement is dependent on the implant engaging the bone surrounding the tooth socket. If patients have insufficient bone around the tooth socket, or if vital structures such as the maxillary sinus or inferior dental nerve are located close to the intended implant site, insertion of an immediate implant will not be possible. These standard-sized implants do not fit the shape of the socket exactly, hence a lack of intimate contact with surrounding alveolar bone is likely to compromise initial implant stability. Under such circumstances, patients will need to undergo bone grafting for delayed implant placement. Having an intimate adaptation of the implant against its bony socket walls is important for promoting primary stability and osseointegration in the longer term. In this study, our aim is to investigate the geometric accuracy of the 3D printed dental implant using a monkey maxilla incisor model. Our goal is to identify the potential sources of error in geometrical accuracy for the development of patient-specific 3D printed dental implants that mimic patient's tooth anatomy.

2. Methods

2.1. Animals and ethics approval

The animal experimental protocol was approved by the Institutional Animal Care and Use Committee of SingHealth, Singapore (IACUC #2018/SHS/1419). The animal laboratory is certified by the International Association for the Assessment of Laboratory Animal Care.

2.2. Segmentation

PET-CT DICOM images of the animals' maxillofacial region were taken and then imported into Mimics inPrint 2.0 software (Materialize) for segmentation of the target central upper incisor from the maxilla (n = 14). First, the "brush threshold" tool was adjusted to 300 – 5000 HU and used to manually select the area within the boundary of the target tooth in each individual sagittal cross-section of the tooth at a contrast of -500 (minimum) to 3000 (maximum). Next, the volume selected was refined by filling up any holes or removing any voxels that fall out of the boundary of the tooth using the "brush erase" tool on each of the frontal and transverse cross-sections. The final volume of the target tooth was then exported to ProPlan CMF 3.0 software for further segmentation. The region of interest spans from 1 mm beneath the cemento-enamel junction to the tooth root (**Figure 1**). This region, termed as the dental implant, was exported as STL data and sent for 3D printing (n = 14).

2.3. Optimisation

To improve consistency in the segmentation process, the contrast and threshold parameters were standardized. A professional digital dentistry personnel was tasked to

perform a segmentation of the same tooth three times and the average of the three parameters was used as the standard.

3D Shape Convince software was used to evaluate the accuracy of the segmentation and printing process. The extracted tooth and 3D printed dental implant were scanned using a micro-CT and converted into an STL format. This was compared against the original STL file that was used to print the dental implant. The overall accuracy of both processes was evaluated by aligning the two STL models using the software's best fit algorithm, then comparing the percentage of the surface area that deviates within a ± 0.1 mm tolerance limit. For the segmentation process, the original segmented STL was compared against the actual tooth model. For the L-PBF process, the printed tooth was compared against the original STL. The overall accuracy of the entire fabrication process was evaluated by comparing the printed tooth to the actual tooth ($n = 8$ as only 8 teeth were extracted from the tooth socket).

2.4. L-PBF fabrication

In this study, the fabrication of actual samples using STL files obtained from the segmentation described

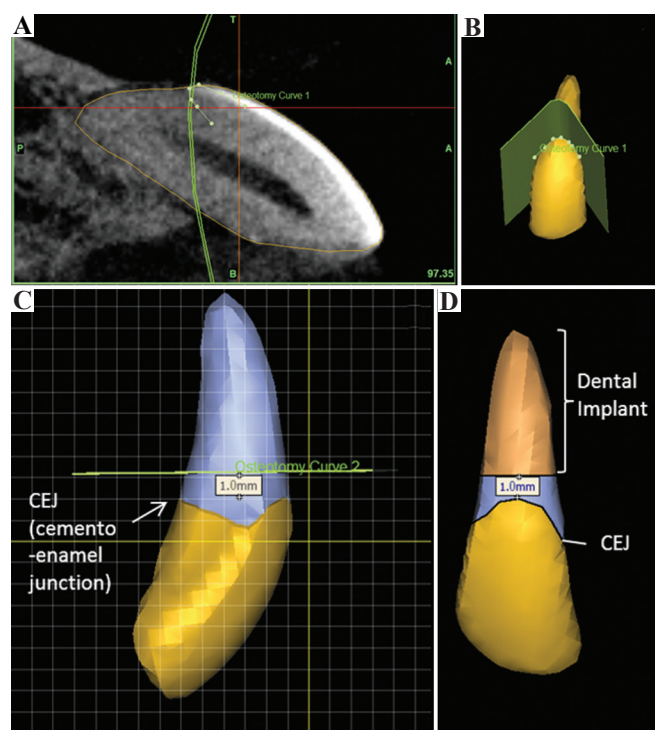


Figure 1. Segmentation of dental implant from a tooth model of the maxilla. (A) Segmentation of tooth along the cemento-enamel junction (CEJ) based on the computed tomography scan (yellow outlined area). (B) Outline of CEJ on tooth model. (C) Plane of segmentation (represented by green line) 1.0 mm above the CEJ. (D) Model of segmented dental implant.

in previous sections was carried out using a SLM 280 HL machine from SLM Solutions AG, Germany. The machine was equipped with a Gaussian beam fiber laser with maximum power of 400 W and a focal diameter of 80 μm . All processing occurred in an argon environment with $<0.05\%$ oxygen to prevent oxidation and degradation of the material during the process. The material used was commercially pure titanium powder (Grade 2 ASTM B348, LPW Technology Ltd, United Kingdom). The powder was spherical in shape and had particle size with average of 43.5 μm . The processing parameters used are summarised in **Table 1**. A stripe scanning strategy was used with stripe width 10.0 mm. A schematic of the scanning pattern is shown in **Figure 2**.

To ensure that the geometry of the fabrication samples was not due to the L-PBF process, preliminary studies were carried out to obtain the correction factor for the L-PBF process. In these preliminary studies, cones with dimensions 4 mm \times 5 mm \times 8 mm were fabricated. The schematic of the samples fabricated is shown in **Figure 3**. The results are tabulated in **Table 2**. The correction factor with least deviations (0.996) is applied for the fabrication of the specimens.

3. Results

The 3D printed dental implant was fabricated based on the STL files obtained from the segmentation of the monkey incisor from its maxilla, then compared against the extracted tooth (**Figure 4**). The 3D printed dental implant measured approximately 1 cm along its entire length.

Overall, our findings showed that the fabrication process produced a 3D printed dental implant that achieved $68.70\% \pm 5.63$ ($n = 8$) accuracy compared to the actual tooth. This implant fabrication was based on the 3D segmented tooth model that had a relatively similar level of accuracy of $66.91\% \pm 10.51$ ($n = 14$) during the segmentation process (**Table 3 and Table S1**). It was noted that the main regions of inaccuracies were at the tooth apex (blue colored zones) (**Figure 5**).

The L-PBF process had a $90.59\% \pm 4.75$ accuracy ($n = 8$) (**Table 3**). The deviation between the RAI and the

Table 1. Process parameters used in L-PBF for fabrication of samples

Process parameters	
Laser power (W)	275
Laser scan speed (mm/s)	1100
Layer thickness (μm)	30
Hatch spacing (mm)	0.120
Fill Contour Offset (mm)	0.06
Boards (mm)	0.09
Remelting	No

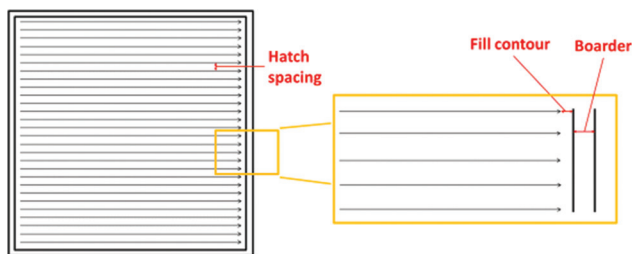


Figure 2. Stripe scanning strategy used in L-PBF shows the fill contour and boarder offset, as well as the hatch spacing which is the distance between the two adjacent laser scan tracks.

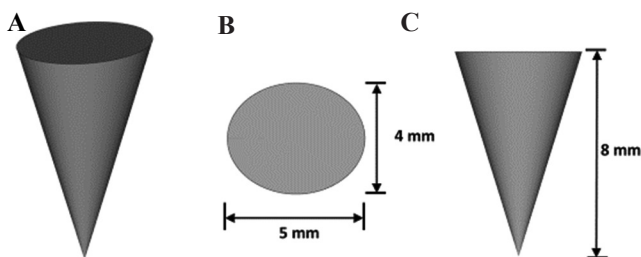


Figure 3. Sample design used for preliminary studies to obtain the correction factor. (A) Isometric view. (B) Top view. (C) Side view.



Figure 4. Extracted monkey incisor and the 3D-printed dental implant, with their respective dimensions.

real tooth can be attributed to the use of support structures at the incisal edge of the RAI during the L-PBF process. These support structures were removed subsequently before the comparison, which may result in inaccuracy at the particular area^[13].

- (a) Overall Group - Printed versus Actual Tooth
- (b) Printed Group - Segmented versus Printed Tooth
- (c) Segmentation Group - Segmented versus Actual Tooth

4. Discussion

The general workflow in using patient-specific dental implants is shown in **Figure 6**. Using the workflow, we identified the major steps in obtaining customized dental implants and studied the potential sources of error in the geometrical accuracy. The stages can be broadly categorized into the “implant design” stage which includes

Table 2. Dimensions of samples obtained from L-PBF with different correction factors

Correction Factor	Length (mm)	Width	Height
0.996	4.02±0.02	5.01±0.02	8.05±0.00
0.998	4.07±0.02	5.05±0.03	8.07±0.02
1.000	4.04±0.04	5.07±0.04	8.10±0.03
1.002	4.05±0.03	5.09±0.02	8.08±0.02
1.004	4.02±0.02	5.08±0.05	8.08±0.04

Table 3. Percentage accuracy of samples in the three different groups

Group Comparison	Accuracy (%)	Min (%)	Max (%)
Overall group (Printed versus actual tooth)	68.70%±5.63	-0.53±0.24	0.32±0.07
Printed group (Segmented versus printed tooth)	90.59%±4.75	-0.12±0.10	0.27±0.06
Segmentation group (Segmented versus actual tooth)	66.91%±10.51	-0.53±0.25	0.50±0.17

the additional imaging, segmentation, optimization of these steps and the “3D printing” stage that involves STL file preparation, the fabrication process, and post-processing which may include polishing, safety testing, and evaluation and finally, implant approval.

Our results showed 66.9% accuracy in the segmentation process, which directly influenced the accuracy of the fabricated implant. To test the fitting of the 3D-printed dental implant within the monkey’s tooth socket, we performed a preliminary study and observed a slight protrusion of the 3D printed dental implant from the socket. This observation corroborated our accuracy study, suggesting that this level of accuracy is likely insufficient and will require further optimization to the segmentation and fabrication methodology to achieve a complete insertion of the 3D printed dental implant into the tooth socket.

Having an intimate and stable fit of the implant within the bone defect region is one of critical factors contributing to primary stability of the dental implant. Other factors such as bone quantity and quality, implant design, surgical technique, and insertion torque also influence the long-term clinical success of the dental implant treatment^[21,22]. Without good biomechanical stability upon implant insertion, osseointegration will not occur^[12]. The term, osseointegration, refers to a direct

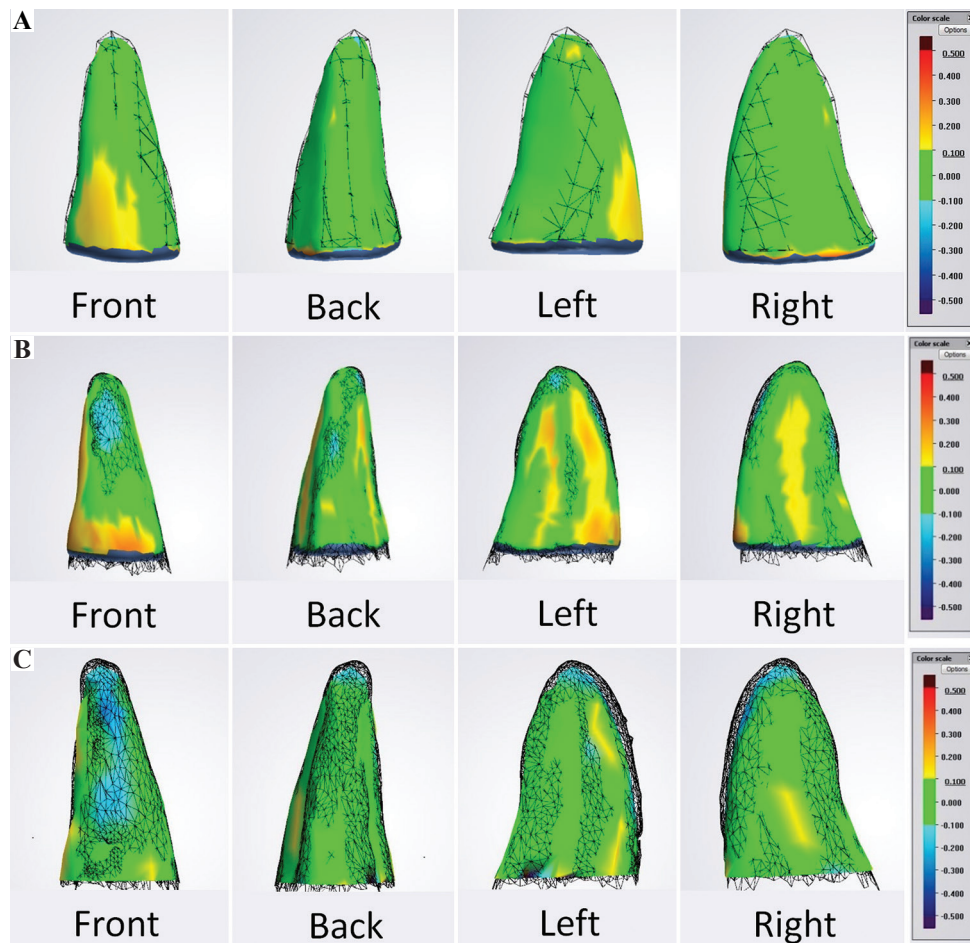


Figure 5. (A) Overall Group - Printed versus Actual Tooth. An example of the front, back, left and right views of the differences in topology of a 3D-printed tooth (solid) against the segmented tooth model (wireframe). (B) Printed Group - Segmented versus Printed Tooth. An example of the front, back, left and right views of the differences in topology of a printed tooth (solid) against the actual tooth (wireframe). (C) Segmentation Group - Segmented versus Actual Tooth. An example of the front, back, left and right views of the differences in topology of a segmented tooth model (solid) against the actual tooth (wireframe). Green represents a high accuracy at which the topology of the two models differs within a ± 0.1 mm tolerance.

structural and functional connection between the bone and implant surface^[23], and was coined by Brånemark in 1977 when he first showed clinical success of the oral implant in his patient due to direct bone-to-implant anchorage^[24,25].

The less-than-desired level of accuracy achieved in this study could be attributed to a few factors. First, the success of image segmentation by thresholding is highly dependent on the skill and experience of the technician and is often based on a subjective interpretation which may result in inter-person variations. The resolution of the scans, particularly at the tooth apex, may also be insufficient and further limited by the allowable threshold tolerance of the software during file import. In addition, the monkey incisor tooth root was small and made it difficult to segment with high accuracy. The bone-tooth densities being different also required different levels of threshold during segmentation. There are also other

commonly cited technical challenges such as irregular anatomical shapes and surfaces, heterogeneous pixel intensities, and noisy boundaries that make it difficult to clearly delineate areas of interest. Hence, any inaccurate image processing will result in deviation error from the planned treatment and desired outcome^[26]. Future work could consider the use of artificial intelligence (AI) tools for medical image segmentation to overcome inter-technician variations, provide higher consistency and performance outcomes, and improve product quality^[27,28] through automated segmentation, rather than manual segmentation by a human. With the large variability of tooth shapes and sizes of different patients, the use of AI for prediction of optimal process parameters would provide greater efficiency, consistency, and cost-savings for mass production and widespread clinical implementation^[10].

Specific to the fabrication and use of custom-made RAI, a few groups have described successful outcomes

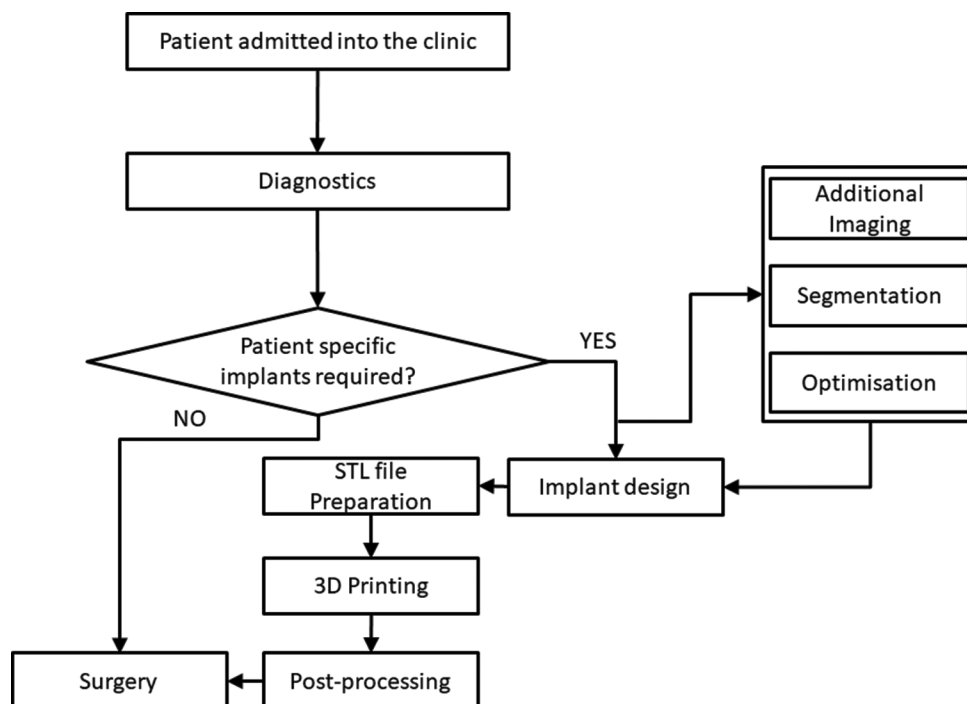


Figure 6. A generic workflow for using patient-specific implants in dental applications.

from preclinical and clinical studies. In a study by Li *et al.*^[29], CP-Ti (Grade 1) SLM-RAI were implanted in two beagle mandibles and its efficacy was compared against the commercial dental screw-type implant. Comparable implant osseointegration was noted *in vivo*, with the added advantage of SLM-RAI being able to significantly reduce the healing time and pain. Figliuzzi *et al.*^[12] demonstrated the successful clinical use of a custom-made Ti-6Al-4V alloy RAI. Fabricated using the direct laser metal forming method, the implant was placed into the maxillary premolar tooth socket immediately upon extraction and restored with a single crown. At 1-year, functional and esthetic integration of the implant was observed. These studies have shown promising results and demonstrate the potential of fabricating custom-made metallic RAI for immediate implantation.

We foresee that this approach will be well-adopted by the various key stakeholders, particularly for patients who are deemed unsuitable for immediate implant placement using conventional dental implants. Patients may now receive treatment using this customized dental implant that allows intimate bone-implant contact for improved primary stability, without having to create a bore hole in their alveolar bone nor face potential surgical risks of encroaching or injuring vital structures.

5. Conclusions

This study studied the accuracy of a titanium dental implant design during the segmentation and 3D printing processes. The goal is to develop an accurate and optimal

workflow methodology to support the fabrication of patient-specific 3D printed titanium dental implants that can mimic patient's tooth anatomy and fit precisely within the socket upon tooth extraction. The use of AM combined with scanning and imaging technologies for customized fabrication of metal implants to meet individual patients' needs is promising and will likely change the business logistics of the current medical implant industry in the future^[5]. However, the use of 3D printing metal implants for biomedical applications is still in its infancy and more research and clinical studies will need to be done to establish the methodologies of 3D printing techniques and understand the long-term safety and clinical efficacy of 3D printed implants. Specific to dental implants, there remains a huge gap between the current conventionally milled dental implants and 3D printed dental implants and more investigations will need to be performed prior to widespread clinical use. Future work will include looking into the performance of the 3D printed metal dental implants, structural characteristics, and the optimization of the L-PBF process in order to achieve better accuracy and performance. Some of the consideration factors for L-PBF include build orientations, process parameters as well as scanning strategies used which have been shown to have an effect on part performance.

Acknowledgments

The authors would like to acknowledge the Digital Dentistry Unit in National Dental Centre Singapore for their support with the use of the softwares.

Funding

This work is funded by the National Health Innovation Centre Singapore (NHIC-I2D-1712189) and National Research Foundation, Prime Minister's Office, Singapore under its Medium-Sized Centre funding scheme.

Conflict of interest

The authors declare no conflict of interest.

Author contributions

G.B.T. and Y.W.Y. guided and supervised the project. All authors contributed to the design of the experiments. L.Y.C., S.S.L. and L.R. conducted the experiments, acquired and analysed the data. L.Y.C., S.S.L., Y.W.Y. and G.B.T. drafted and revised the manuscript.

References

1. Tofail SA, Koumoulos EP, Bandyopadhyay A, *et al.*, 2018. Additive Manufacturing: Scientific and Technological Challenges, Market Uptake and Opportunities. *Mater Today*, 21:22–37.
<https://doi.org/10.1016/j.mattod.2017.07.001>
2. Ryan G, Pandit A, Apatsidis DP, 2006. Fabrication Methods of Porous Metals for Use in Orthopaedic Applications. *Biomaterials*, 27:2651–70.
<https://doi.org/10.1016/j.biomaterials.2005.12.002>
3. Bose S, Roy M, Bandyopadhyay A, 2012. Recent Advances in Bone Tissue Engineering Scaffolds. *Trends Biotechnol*, 30:546–54.
<https://doi.org/10.1016/j.tibtech.2012.07.005>
4. Bai CG, Chen X, Sun Y, *et al.*, 2019. Additive Manufacturing of Customized Metallic Orthopedic Implants: Materials, Structures, and Surface Modifications. *Metals*, 9:1004.
<https://doi.org/10.3390/met9091004>
5. Ni J, Ling H, Zhang S, *et al.*, 2019. Three-dimensional Printing of Metals for Biomedical Applications. *Mater Today Bio*, 3:100024.
<https://doi.org/10.1016/j.mtbio.2019.100024>
6. Lowther M, Louth S, Davey A, *et al.*, 2019. Clinical, Industrial, and Research Perspectives on Powder bed Fusion Additively Manufactured Metal Implants. *Addit Manuf*, 28:565–84.
<https://doi.org/10.1016/j.addma.2019.05.033>
7. Sing SL, An J, Yeong WY, *et al.*, 2016. Laser and Electron-beam Powder-bed Additive Manufacturing of Metallic Implants: A Review on Processes, Materials and Designs. *J Orthop Res*, 34:369–85.
<https://doi.org/10.1002/jor.23075>
8. Sing SL, Huang S, Goh GD, *et al.*, 2021. Emerging Metallic Systems for Additive Manufacturing: In-situ Alloying and Multi-metal Processing in Laser Powder Bed Fusion. *Prog Mater Sci*, 119:100795.
<https://doi.org/10.1016/j.pmatsci.2021.100795>
9. Wu H, Ren Y, Ren J, *et al.*, 2020. Effect of Melting Modes on Microstructure and Tribological Properties of Selective Laser Melted AlSi10Mg Alloy. *Virtual Phys Prototyp*, 15:570–82.
<https://doi.org/10.1080/17452759.2012.673152>
10. Sing SL, Kuo CN, Shih CT, *et al.*, 2021. Perspectives of Using Machine Learning in Laser Powder Bed Fusion for Metal Additive Manufacturing. *Virtual Phys Prototyp*, 16:372–86.
<https://doi.org/10.1080/17452759.2021.1944229>
11. Chahal V, Taylor RM, 2020. A Review of Geometric Sensitivities in Laser Metal 3D Printing. *Virtual Phys Prototyp*, 15:227–41.
<https://doi.org/10.1080/17452759.2019.1709255>
12. Figliuzzi M, Mangano F, Mangano C, 2012. A Novel Root Analogue Dental Implant Using CT Scan and CAD/CAM: Selective Laser Melting Technology. *Int J Oral Maxillofac Surg*, 41:858–62.
<https://doi.org/10.1016/j.ijom.2012.01.014>
13. Moin DA, Hassan B, Parsa A, *et al.*, 2012. Accuracy of Preemptively Constructed, Cone Beam CT-, and CAD/CAM Technology-based, Individual Root Analogue Implant Technique: An *In Vitro* Pilot Investigation. *Clin Oral Implants Res*, 25:598–602.
<https://doi.org/10.1111/clar.12104>
14. Moin DA, Hassan B, Mercelis P, *et al.*, 2011. Designing a Novel Dental Root Analogue Implant Using Cone Beam Computed Tomography and CAD/CAM Technology. *Clin Oral Implants Res*, 24:25–7.
<https://doi.org/10.1111/j.1600-0501.2011.02359.x>
15. Chen J, Zhang Z, Chen X, *et al.*, 2014. Design and Manufacture of Customized Dental Implants by Using Reverse Engineering and Selective Laser Melting Technology. *J Prosthet Dent*, 112:1088–95.e1081.
<https://doi.org/10.1016/j.prosdent.2014.04.026>
16. Li J, Hu J, Zhu Y, Yu X, *et al.*, 2020. Surface Roughness Control of Root Analogue Dental Implants Fabricated Using Selective Laser Melting. *Addit Manuf*, 34:101283.
<https://doi.org/10.1016/j.addma.2020.101283>
17. Li XC, He L, Zhang JW, *et al.*, 2021. Additive Manufacturing of Dental Root-Analogue Implant with Desired Properties. *Mater Technol*, 36:894–906.
<https://doi.org/10.1080/10667857.2020.1859054>

18. Guo F, Hu M, Wang C, *et al.*, 2020. Studies on the Performance of Molar Porous Root-Analogue Implant by Finite Element Model Simulation and Verification of a Case Report. *J Oral Maxillofac Surg*, 78:e1961–5.e9.
<https://doi.org/10.1016/j.joms.2020.06.002>
19. Song K, Wang Z, Lan J, *et al.*, 2021. Porous Structure Design and Mechanical Behavior Analysis Based on TPMS for Customized Root Analogue Implant. *J Mech Behav Biomed Mater*, 115:104222.
<https://doi.org/10.1016/j.jmbbm.2020.104222>
20. Bhola M, Neely AL, Kolhatkar S, 2008. Immediate Implant Placement: Clinical Decisions, Advantages, and Disadvantages. *J Prosthodont*, 17:576–81.
<https://doi.org/10.1111/j.1532-849X.2008.00359.x>
21. Friberg B, Jemt T, Lekholm U, 1991. Early Failures in 4,641 Consecutively Placed Branemark Dental Implants: A Study from Stage 1 Surgery to the Connection of Completed Prostheses. *Int J Oral Maxillofac Implants*, 6:142–6.
22. Cobo-Vazquez C, Reininger D, Molinero-Mourelle P, *et al.*, 2018. Effect of the Lack of Primary Stability in the Survival of Dental Implants. *J Clin Exp Dent*, 10:e14–9.
<https://doi.org/10.4317/jced.54441>
<https://doi.org/10.1016/j.ijom.2012.01.014>
23. Albrektsson T, Albrektsson B, 1987. Osseointegration of Bone Implants. A Review of an Alternative Mode of Fixation. *Acta Orthop Scand*, 58:567–77.
<https://doi.org/10.3109/17453678709146401>
24. Branemark PI, Hansson BO, Adell R, *et al.*, 1977. Osseointegrated Implants in the Treatment of the Edentulous Jaw. Experience from a 10-Year Period. *Scand J Plast Reconstr Surg Suppl*, 16:1–132.
25. Albrektsson T, Branemark PI, Hansson HA, *et al.*, 1981. Osseointegrated Titanium Implants. Requirements for Ensuring a Long-lasting, Direct Bone-to-implant Anchorage in Man. *Acta Orthop Scand*, 52:155–70.
26. Wong KC, 2016. 3D-printed Patient-specific Applications in Orthopedics. *Orthop Res Rev*, 8:57–66.
<https://doi.org/10.2147/ORR.S99614>
27. Meng L, McWilliams B, Jarosinski W, *et al.*, 2020. Machine Learning in Additive Manufacturing: A Review. *J Min Metals Mater Soc*, 72:2363–77.
<https://doi.org/10.1007/s11837-020-04155-y>
28. Ng WL, Chan A, Ong YS, *et al.*, 2020. Deep Learning for Fabrication and Maturation of 3D Bioprinted Tissues and Organs. *Virtual Phys Prototyp*, 15:340–58.
<https://doi.org/10.1080/17452759.2020.1771741>
29. Lia JH, Zhu Y, Yu X, *et al.*, 2020. Surface Roughness Control of Root Analogue Dental Implants Fabricated Using Selective Laser Melting. *Addit Manuf*, 34:101283.
<https://doi.org/10.1016/j.addma.2020.101283>

Publisher's note

Whoice Publishing remains neutral with regard to jurisdictional claims in published maps and institutional affiliations.